Check for updates

Modeling the formation and thermomechanical properties of polybenzoxazine thermosets†

Shamil Saiev,[a] Leïla Bonnaud,[b] Philippe Dubois,[a,c] David Beljonne [ID][a] and Roberto Lazzaroni [ID] *[a]

We present a comparative molecular modeling study of the thermomechanical properties of crosslinked benzoxazine resins. A crosslinking algorithm was developed in order to simulate the thermal curing of thermoset resins and monitor the evolution of their network topology. The resin properties (gelation point, crosslink density, volumetric expansion, glass transition temperature, thermal expansion coefficient and elastic constants) were probed as a function of the network composition. The simulation results are in line with analytical models and in very good agreement with experimental data. Our molecular dynamics simulations provide a detailed rationale for the differences in the measured thermomechanical properties of recently reported benzoxazine derivatives and pave the way to the design of improved resins using predictive modeling tools based on the monomer chemical structure as the sole input.

1 Introduction

Thermoset resins are used for a wide range of applications due to their high mechanical strength, processability, dimensional stability and relatively low cost. Epoxy and phenolic resins are the classical representatives of thermosets which for a long time have played a key role in diverse industrial fields starting from household materials to high-technology aerospace applications. However, these materials suffer from a number of shortcomings such as the use of harsh catalysts for polymerization, poor shelf life, release of volatiles during the curing resulting in a large volumetric shrinkage, micro-void formation and brittleness of the cured resins. Over the last few years, benzoxazine resins have been proposed as a new class of phenolic resins,[1] as these show potential far beyond that of traditional phenolics and epoxies. Benzoxazine resins have major advantages in terms of thermomechanical resistance and flame retardance properties. They also exhibit attractive features such as low water absorption, low thermal expansion, higher char yields, a near-zero volumetric change upon curing, easy thermal curing by ring opening polymerization with no reaction by-products, no catalysts required for curing and in some cases the T_g can be higher than the curing temperature.[2] Benzoxazine monomers can be easily synthesized from phenols, primary amines and formaldehydes, and hence, there is a rich molecular design flexibility to achieve specific properties depending on the desired applications. Moreover, by using renewable building blocks for the preparation of the monomers, it is possible to synthesize partially or fully bio-based benzoxazines; this is a key advantage in both academia and industry since it offers the possibility to reduce the demand for fine chemicals in the production of oils and their derivatives.[3] Bisphenol-A-based benzoxazine (BA-a) is one of the most common members of the family and is commercially available. Even though BA-a thermosets present good intrinsic properties, it appears that irreversible thermal degradation occurs during the curing of the monomer, which leads to the formation of voids in the crosslinked resin.[4] In order to overcome these shortcomings, a new benzoxazine compound based on phenol-*p*-phenylene diamine (P-*p*PDA) has been recently synthesized by a solventless process with negligible thermal degradation and higher thermomechanical properties.[4,5] To complete the study, an additional structure based on 4,4′-(*p*-phenylene)bis(3,4-dihydro-6-ethyl-2*H*-1,3-benzoxazine) (4EP-*p*PDA) has also been prepared. All these monomers are typically bifunctional benzoxazine compounds, as shown in Fig. 1. BA-a is based on bisphenol and mono-amine, whereas P-*p*PDA and 4EP-*p*PDA are based on phenol and aromatic diamines, with the 4EP-*p*PDA monomer having additional ethyl functions attached to the *para* positions of the external benzene rings. The polymerization process for benzoxazine resins is initiated *via* a thermally-induced ring-opening reaction to form a phenolic structure through a Mannich

[a]Laboratory for Chemistry of Novel Materials, University of Mons – UMONS, Place du Parc 20, 7000 Mons, Belgium. E-mail: roberto.lazzaroni@umons.ac.be
[b]Materia Nova R&D Center, Avenue Copernic 1, Parc Initialis, 7000 Mons, Belgium
[c]Laboratory of Polymeric and Composite Materials, University of Mons – UMONS, Place du Parc 20, 7000 Mons, Belgium

†Electronic supplementary information (ESI) available: The effect of the cooling rate and the analysis method for the calculations of the T_g. See DOI: 10.1039/c7py00995j
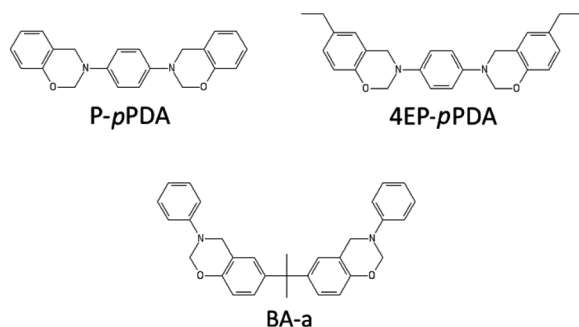
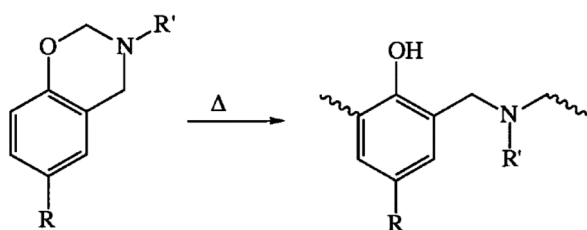**Fig. 1** BA-a, P-*p*PDA and 4EP-*p*PDA structures.

Fig. 2 Polymerization reaction of benzoxazine by the formation of a Mannich Bridge at the *ortho* position.[8]

bridge,[6–8] Fig. 2. In principle, there are three possible reaction sites on the aromatic ring: *ortho*, *para* and *meta* positions. It has been demonstrated that the reaction occurs preferentially on the *ortho* position, although reactions can also occur, yet to a much lesser extent, on the *para* and even the *meta* positions.[8]

In this modeling work, only reactions on the *ortho* position are considered since these reactions are by far predominant.

Molecular dynamics (MD) simulations are becoming increasingly relevant in polymer science as they provide a means to numerically verify the theoretical models, yield additional insight into experimentally-observed properties and predict the performance of new formulations. The initial efforts to model the formation of crosslinked networks can be traced back to the 80's and 90's. In previous studies the network construction was processed through Monte Carlo simulations without considering any chemical detail.[9] Later on, more sophisticated methods were elaborated allowing a fully atomistic representation of polymer networks, by using multi-step procedures that allow repeated creation of covalent bonds and equilibration of the structure until the desired crosslink conversion is reached.[10–12] Computational simulations have also been used in order to simulate the thermomechanical properties such as the glass transition temperature (T_g), heat capacity (C_p), volume expansion coefficient (α_v) and elastic constants.[13–17] Reasonably good agreement was obtained between experiment and theory, demonstrating that atomistic simulations can be an efficient tool to study thermosetting polymers. The influence of the degree of polymerization on the material properties (*e.g.*, T_g and yield stress) has

also been investigated. More recently, Li and Strachan studied the network topology of bifunctional epoxy thermosets in order to highlight the influence of structural defects on the material properties and calibrate the existing predictive models.[18]

Molecular modelling techniques have been employed in order to gain insight into the microstructural properties of polybenzoxazines. In particular, the analysis of single chain spatial structures and supramolecular network structures revealed the role of hydrogen bonding in the crosslinking processes and the overall thermomechanical properties of polybenzoxazine polymers.[19–21] Kim and Mattice have used MD simulations to investigate the conformational distribution of single and bulk chains, the importance of hydrogen bonding, and the structure of thin polybenzoxazine films.[22–25] The thermomechanical properties of these thermosets were studied by Hamerton and Hall *et al.*, showing good agreement with the experiment.[26,27]

In this work, atomistic simulations are used in order to study the crosslinking process of three specific benzoxazines: BA-a, P-*p*PDA and 4EP-*p*PDA, and the properties of the resulting networks. Experimentally the P-*p*PDA thermosets display the best thermostability and mechanical properties at high temperature (as a result of a higher glass transition temperature) among these three polybenzoxazines.[4] We applied MD simulations to gain a fundamental insight into the relationship between the structural network topology and the observed properties of the resins, and to identify the molecular mechanisms responsible for the thermomechanical behaviour of these polybenzoxazines. Following the approach of Li and Strachan, we developed our own algorithm to assess the network topology during the crosslinking process, by quantifying the number of dangling and loop chains and monitoring the overall number and length of elastic chains. We focused on the dependency of the thermomechanical properties of benzoxazine resins on the initial monomer structure and the network topology of the cured systems.

This paper is organized as follows: section 2 contains the details of the MD simulations, including the preparation of structures, the scheme for modeling the crosslinking process, the description of the thermomechanical analysis and topological characterization methods. Section 3 presents the results and related discussions. Finally, we closed this work with concluding remarks in section 4.

2 Experimental

2.1 Resin network construction

MD simulations are carried out with the Materials Studio 7.0 (Accelrys Inc.) package using an optimized version of the Dreiding force field to properly account for inter- and intramolecular interactions.[28] The partial charges on the molecules are obtained from iterative partial equalization of orbital electronegativity using the Gasteiger method.[29] The non-bonded interactions are measured using the Lennard-Jones

(12-6) potential function and group-based summation for van der Waals and electrostatic interactions, respectively, with the cut-off set at 1.2 nm for both types of interactions. The key advantages of the group-based summation are: (i) the reduction of sudden energy fluctuations by avoiding the creation of spurious monopoles when the dipoles are split near the cut-off distance (when one of the dipole atoms is inside the cut-off and another is outside); (ii) the reduction of the computational effort compared to atom-based and Ewald summation methods by creating larger electrically-neutral clusters from different groups of atoms. The temperature of the simulation box is controlled using the Nosé–Hoover–Langevin (NHL) thermostat with a Q ratio of 0.01.[30] This method is shown to be superior in controlling the temperature compared to the original Nosé–Hoover thermostat.[31] For the pressure control in NPT-MD simulations (constant pressure, temperature and number of particles), we used the Parrinello–Rahman barostat since it introduces more degrees of freedom to the system and leads to more natural relaxation of the molecular structures.

All the model systems in this study consist of 200 monomer molecules per simulation box for each studied resin. The crosslinked networks are constructed using the cyclic polymerization atomistic model with controlled multi-step topology relaxation:

(i) at the start of the simulation, the desired number of monomer molecules are inserted into the cubic simulation cell under 3D periodic boundary conditions at a low density (0.6 g cm^{-3}). The system energy is minimized and then equilibrated in the NVT ensemble for 100 ps at 500 K, followed by a NPT simulation for 500 ps at 300 K. The final average box size is ∼5 nm. The obtained simulation density at room temperature is in good agreement with experimental results, Table 1. The average error is 8.0, 6.7 and 3.6% for P-*p*PDA, BA-a and 4EP-*p*PDA, respectively, within the limit of validity for force field simulations (errors smaller than 10% are usually considered as acceptable).

(ii) During the curing, the occurrence of close contacts between the reactive atoms is detected using a distance-based criterion ranging from 0.4 to 0.8 nm. If the distance condition is satisfied, the oxazine cycle is opened by breaking the O–C bond, a new covalent bond is created between the N–C group and the *ortho* carbon of the aromatic ring forming the Mannich bridge. When all possible bonds are created, the system goes through a multistep relaxation–perturbation procedure using the NVT-NPT dynamics and then a new round of bond creation is attempted. This procedure ends when a predefined conversion limit is reached; in this work, a full analysis of the crosslinking system was carried out as a function of the conversion rate, with steps of 10%, up to 90%.

(iii) Linking monomers together leads to progressively larger branched chains. At a certain stage of the reaction, as the linking process proceeds, the largest chain diverges into the "infinite size", spanning the whole system. This infinite molecule is called the gel fraction and all other remaining chains constitute the sol fraction; the situation where the gel first appears is called the gel-point.[32–34] All along the polymerization process, the sizes of the chains present in the system are recorded as a function of the conversion rate, giving access to the molecular characteristics of the system: the number-average molar mass M_n, the weight-average molar mass M_w, the reduced weight-average degree of polymerization (RDP) and the weight fraction of the gel W_g. It must be pointed out that RDP is identical to M_w except for the consideration of the largest molecule in the system. The gel-point can be estimated from these structural characteristics: it corresponds to the maximum of the RDP values and to the inflection point of the M_w curve.[35,36]

The gel fraction contains structural defects such as dangling chains and loops, which do not contribute to the elastic behaviour. Therefore, Scanlan and Case have defined the active part of the gel as being composed of 'active crosslinks' joined by at least three paths to the infinite network and 'active chains' terminated by active crosslinks at both ends.[37,38] In this work, we classify the chains formed during the crosslinking into five types, see Fig. 3: (i) elastically active crosslinks (at least three paths leading to the infinite structure), (ii) active chains (both ends are connected to active crosslinks), (iii) dangling chains (chains attached to the infinite network only by one end), (iv) loops (both ends are connected to the same active junction) and (v) free chains (chains belonging to the sol fraction). The algorithm works as follows:
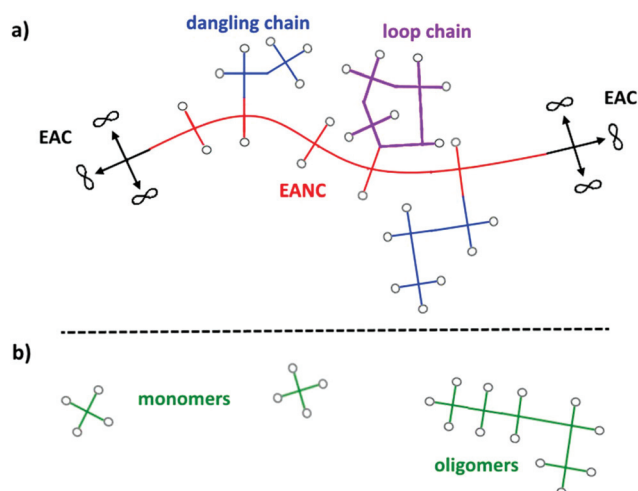

Fig. 3 Polymer network for tetrafunctional branching units. (a) The gel fraction (largest fragment) is composed of: elastically active crosslinks, EACs (black), elastically active network chains, EANCs (red), dangling chains (blue) and loop chains (purple); (b) the sol fraction (green) includes all the monomers and oligomers that are not attached to the largest fragment.

Table 1 Simulated and experimental density for the monomers

	BA-a	P-*p*PDA	4EP-*p*PDA
Sim. density (g cm^{-3})	1.11 ± 0.003	1.16 ± 0.003	1.06 ± 0.003
Exp. density (g cm^{-3})	1.20	1.25	1.10

(i) during curing the new linked pairs of atoms are assigned with the same name; (ii) the linkage map is established by using the names of the reacted atoms between all the molecules in the largest fragment; (iii) the next step is the identification of linear chains and their chain lengths; and (iv) finally, each monomer unit is classified into one of the five categories: active crosslinks, loops, free chains, and elastically active and dangling chains. In order to check the reliability of the algorithm, a complete manual analysis was performed on crosslinked structures with different conversion rates; good agreement was obtained with the algorithm implementation.

2.2 Measurement of the thermomechanical properties

Experimentally, calorimetric studies were carried out at a heating rate of 10 °C min^{-1} using a differential scanning calorimeter (DSC Q200 from TA Instruments) under a nitrogen flow of 50 mL min^{-1}. Indium was used for calibration. The thermomechanical properties were studied by dynamic mechanical thermal analysis (DMA 2980 Dynamical Mechanical Analyzer from TA Instruments). The measurements were performed in a dual cantilever configuration with a length of 35 mm, operating at a frequency of 1 Hz, from 25 to 370 °C at a heating rate of 3 °C min^{-1}, with a displacement of 18 microns corresponding to a strain of 0.043%. One representative sample was used for the measurements.[5]

In the MD simulations, the thermal and volumetric properties of the crosslinked networks were assessed by annealing through a stepwise temperature profile ranging from high to low temperature. T_g is usually defined as the intersection of the linear density–temperature or volume–temperature curves of the glassy and rubbery states. To calculate T_g and other thermodynamic quantities, a high-temperature annealing protocol was followed: the crosslinked structures obtained from the algorithm described above were equilibrated at 850 K for 1 ns in the NPT ensemble under atmospheric pressure, in order to release constraints induced by curing. Afterwards, the structures underwent stepwise cooling from 850 K to 50 K in steps of 50 K for 400 ps. Such a cooling rate is comparable to the values used in previous studies of thermosets[10,12,15,39] and we have tested that the relaxation of the polybenzoxazine systems occurs sufficiently fast, so that the T_g values are not affected by the cooling rate (see an example in Fig. S2†). The temperature, volume, valence energies, non-bonded energies as well as the structural characteristics were averaged and stored for further analysis.

The mechanical properties of the fully crosslinked polymers (90% conversion) were measured using the constant-strain or static approach implemented in Materials Studio.[40] During the annealing procedure, and after an equilibration step at 300 K, the structures were extracted and stored for further analysis of the mechanical properties. The measurement is initiated by pre-minimizing the system in order to bring it closer to the lowest energy configuration. Three tensile and three shear deformations of a small amplitude are then applied to the simulation box in all directions, followed by energy minimization. The maximum strain amplitude is set to 0.002 and 6

strain steps are applied along every strain direction. The resulting distorted structures are re-optimized keeping the cell parameters fixed, and then the internal stress tensor is obtained using the virial expression. The stiffness matrix is built up by estimating the first derivatives of the virial stress components with respect to strain ($\partial\sigma/\partial\varepsilon$). From the obtained matrix, the Lamé coefficients (λ and μ) are calculated as follows:

$$\mu = \frac{1}{3}(C_{44} + C_{55} + C_{66}) \tag{1}$$

$$\lambda + 2\mu = \frac{1}{3}(C_{11} + C_{22} + C_{33}) \tag{2}$$

By making an assumption that the molecular structure is like that of the isotropic material, the stiffness matrix can be defined as follows:

$$\begin{pmatrix} \lambda + 2\mu & \lambda & \lambda & 0 & 0 & 0 \\ \lambda & \lambda + 2\mu & \lambda & 0 & 0 & 0 \\ \lambda & \lambda & \lambda + 2\mu & 0 & 0 & 0 \\ 0 & 0 & 0 & \mu & 0 & 0 \\ 0 & 0 & 0 & 0 & \mu & 0 \\ 0 & 0 & 0 & 0 & 0 & \mu \end{pmatrix} \tag{3}$$

In the isotropic case, the elastic properties can thus be fully described by using these two independent Lamé coefficients and by applying linear elasticity theory:

$$E = \frac{\mu(3\lambda + 2\mu)}{\lambda + \mu} \tag{4}$$

$$K = \lambda + \frac{2}{3}\mu \tag{5}$$

$$G = \mu \tag{6}$$

$$\upsilon = \frac{\lambda}{2(\lambda + \mu)} \tag{7}$$

where E, B, G and υ are the Young's, bulk and shear moduli and Poisson's ratio, respectively.

3 Results and discussion

3.1 Network topology

The algorithm described above enables us to track the changes of the network topology at various degrees of conversion. Fig. 4 shows the weight percent evolution of free, dangling, loop and elastic chains present in the structures as a function of the conversion rate. As expected, as the curing proceeds, the number of free chains keeps decreasing until they completely disappear above 80% of conversion for all resins. The elastic chains (elastically active crosslinks and chains) appear after the largest fragment becomes infinite with the formation of the first active crosslink; from these data we can roughly estimate that the gel-point for all resins is located between 40 and 50% of the conversion rate. The structural defects, *i.e.*, dangling and loop chains, peak in the region of the gel-point, then progressively decrease and eventually disappear at 90% of conversion. It is important to point out that structural
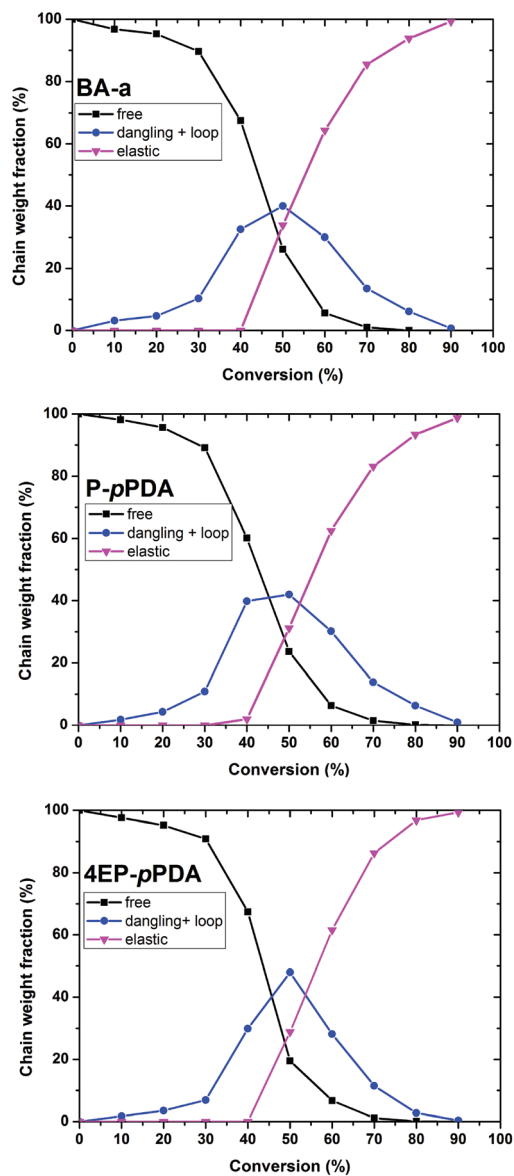
Fig. 4 Percent molecular weight of free, dangling, loop and elastic chains as a function of the conversion rate for BA-a, P-*p*PDA and 4EP-*p*PDA.

defects make physical sense only when attached to the infinite structure. Therefore, the increase of the dangling and loop chains below the gel-point reflects the growth of the largest fragment rather than the formation of structural defects in the resins.

As the crosslinking proceeds, the weight of elastic chains increases by consuming dangling, loop and free chains. At 90% the systems are considered to be ideal structures, with all the chains contributing to the elastic behaviour of the cross-linked resins.

We also measured the density of elastically active chains v_e (also called the crosslink density) as the ratio of the number of EANCs to the volume of the simulation box. Experimentally,

v_e can be estimated by measuring the equilibrium modulus in the rubbery state at temperature T_g + 40 °C and applying the molecular rubber elasticity theory:[41]

$$G = \varphi \frac{NKT}{V} = \varphi v_e KT \qquad (8)$$

where G is the elastic modulus, N is the number of elastically active chains, K is the Boltzmann's constant, T is the absolute temperature, V is the volume, v_e is the crosslink density and φ is the front factor, which is unity for ideal rubbers. Li and Strachan in their work calculated the values of the crosslink density of their polymers by taking into account the amount of structural defects.[18]

Fig. 5 shows the evolution of v_e, the gel fraction W_g and RDP as a function of the conversion rate for the three studied resins. On the one hand, it has already been pointed out that the appearance of the first elastic chains and the maximum of RDP correspond to the gel-point; on the other hand, Flory has demonstrated that the rapid increase of the gel fraction corresponds to the gelation as well.[34] From these three approaches, the most accurate one is the emergence of the crosslink density v_e since the most basic condition for gelation is the presence of the infinite network. However, due to the computational limitations, the crosslink density is measured only for certain values of the conversion rate, with 10% resolution. As a result, we cannot estimate the exact gel-point from the measured crosslink density. In the case of BA-a and 4EP-*p*PDA resins, the appearance of the first elastic chain is somewhere between 40 and 50% of conversion, whereas for P-*p*PDA there are elastic chains already at a 40% conversion rate. The maximum of the RDP curve helps to calculate more accurate gelation values for these resins; here it is estimated to be 44.4 ± 0.9% for BA-a, 40.3 ± 2.5% for P-*p*PDA and 43.8 ± 3.7% for 4EP-*p*PDA. This is consistent with the sudden increase of the gel fraction W_g at the calculated gel-point. The RDP and W_g values are in agreement with the appearance of the first elastically active chains in the structures, which further supports the validity of the algorithm. For the fully crosslinked benzoxazine networks, the crosslink density is found to be in the range of 2.6–3.63 × 10^{-3} mol cm^{-3}, which is below the reported values for epoxy resins (~6.6 × 10^{-3} mol cm^{-3}).[42] In the same paper, the crosslink density of BA-a is measured to be 1.1 × 10^{-3} mol cm^{-3}, which is below the value for the fully cured BA-a resin calculated from these simulations. This difference is probably related to the partial thermal degradation of BA-a during curing, which reduces the experimental crosslink density compared to the ideal case. As shown in Fig. 4, the systems have only a small amount of free chains and structural defects at a conversion degree of above 80%. This is directly related to the poor increase of the crosslink density at high conversion rates since almost all the structural chains are elastically active.

It is important to note that even though these three molecules have the same nature and the same number of functional sites, the calculated gel point differs for P-*p*PDA compared to BA-a and 4EP-*p*PDA. This can be attributed to the
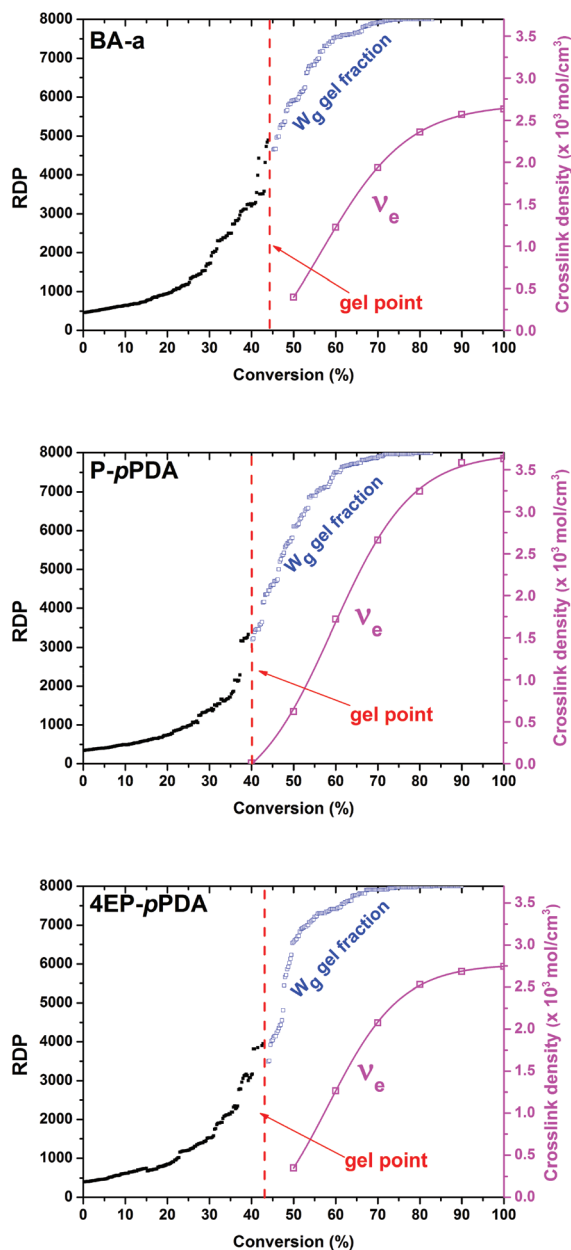
Fig. 5 Evolution of the reduced weight-average degree of polymerization (RDP), crosslink density and gel-fraction as a function of the conversion degree for BA-a, P-*p*PDA and 4EP-*p*PDA.

below the gel-point is around 3% for all resins; the remaining over-estimation is thus related to the actual geometry of the molecules resulting in the different steric accessibility of the functional atoms.

Another widely used molecular characteristic of crosslinked polymers is the average molecular weight between crosslink sites M_c in the gel. It is related to the crosslink density through the mass density: $M_c = \rho/\nu_e$.[18] This equation is valid only for high degrees of conversion when all the chains are supposed to be elastically active, since it is experimentally impossible to evaluate the number of structural defects in the polymer. Fig. 6 shows the number average molecular weight of all the chains M_n and M_c as a function of the conversion degree for the three resins. By definition, M_n represents the average chain weight of all the fragments below the gel-point; it increases as monomers react with each other forming larger fragments, until the gelation is reached. M_c is calculated above the gel-point and represents the average molecular weight between the active crosslinks in the largest fragment; it can be defined only after gelation when the first elastically active crosslinks appear in the system. Just above the gel-point, M_c shows its maximum value and it decreases progressively with increasing conversion rate as more chains become crosslinked and the average chain length between crosslinks becomes shorter. M_n and M_c are similar for all studied resins; the weight difference is attributed to different monomer molecular weights, namely 462.6 g mol^{-1} for BA-a, 344.4 g mol^{-1} for P-*p*PDA and 400.5 g mol^{-1} for 4EP-*p*PDA. It can be seen that at 90% conversion, M_c reaches the monomer molar mass indicating that the fully crosslinked structures are composed mostly of elastically active crosslinks.

3.2 Glass transition and thermal expansion

Fig. 7(a) and (b) illustrate the density *versus* temperature plots and the coefficient of volume thermal expansion α_v for conversion rates increasing from 0 to 80% for P-*p*PDA (all three resins exhibit similar trends, see the ESI†). T_g is marked by the discontinuity of the density–temperature curve slope; it is cal-
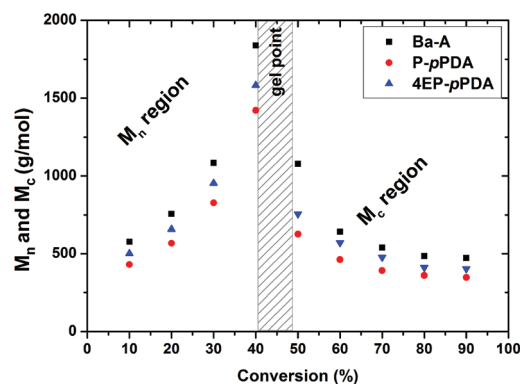
difference in the monomer structures, which affects the steric accessibility of the reactive sites (it is expected to be easier in P-*p*PDA) and the associated free volume in the system. It is also noteworthy that the gel-point values for all resins are higher than the theoretical gel-point for tetra-functional molecules (33%) calculated using Flory's model of critical conversion for an ideal crosslinking process. In that model, the geometrical constraints and the intra-chain reactions likely to occur during curing are not taken into account.[32] In contrast, these phenomena are present in our simulations and affect the gelation process. The amount of intra-molecular crosslinks

Fig. 6 Number average molecular weight before the gel-point (M_n) and average weight of chains between crosslinks (M_c) after the gel-point as a function of the conversion degree.
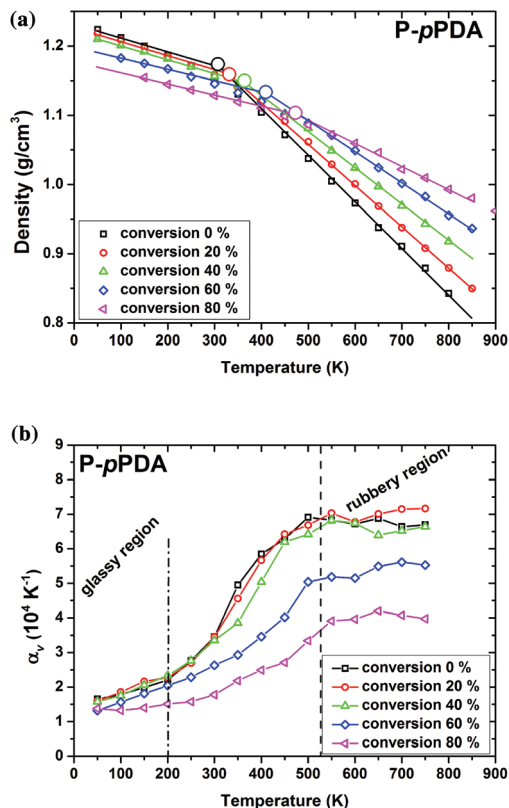
Fig. 7 (a) Density as a function of the conversion degree for P-pPDA. The open circles indicate the value of T_g. (b) Coefficient of volume thermal expansion (α_v) for the glassy and rubbery states for P-pPDA.

culated as the intersection of two linear plots fitted to the density values in the low and high temperature regions, respectively. The existence of the linear regimes can be confirmed by calculating the coefficient of volume thermal expansion α_v:

$$\alpha_v = \frac{1}{V_0}\frac{\partial V}{\partial T} \tag{9}$$

where V_0 is the reference volume at 300 K and $\partial V/\partial T$ is the first-order derivative of the volume–temperature curve. Fig. 7(b) shows the thermal coefficient values as a function of conversion for P-pPDA. Three general regimes of α_v can be observed for all conversion rates: (i) at low temperature, α_v is small and weakly increasing; this corresponds to the glassy region, (ii) the transition region is marked by the strong increase of α_v in the intermediate temperature range, and (iii) at high temperatures, α_v is large and constant, corresponding to the rubbery region.

The T_g values as a function of the conversion rate (0 to 90%) are shown in Fig. 8 for the three resins. For P-pPDA, T_g varies from 37 °C in the monomer to 216 °C at maximum conversion, in very good agreement with the experimental results: 45 °C for uncured monomers and 220 °C for the fully cross-linked resin.[5] In the case of 4EP-pPDA, the calculated T_g increases from 47 °C to 150 °C, the latter result also being in
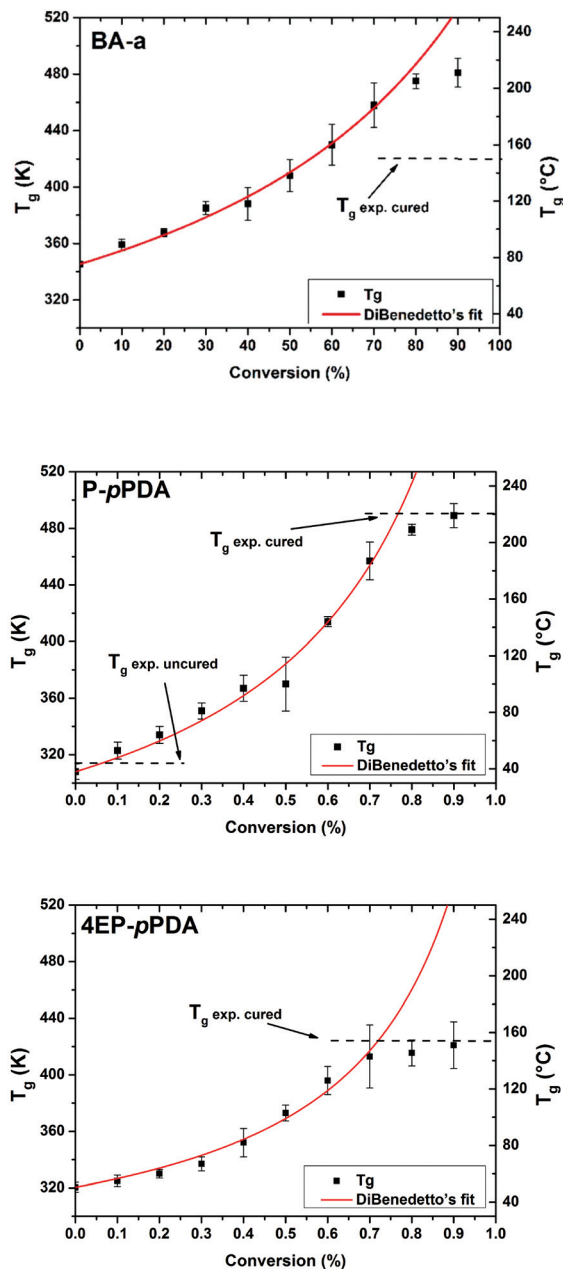

Fig. 8 Glass transition temperature as a function of the conversion degree with the corresponding experimental values for BA-a, P-pPDA and 4EP-pPDA. The values in Table 3 are the results of a fit using Di Benedetto's equation.

excellent agreement with the experimental T_g for the cured resin (155 °C) and in the range expected for epoxy resins (165 °C).[42] The mechanisms involving the glass transition of thermosets are somewhat complex; in the case of epoxy resins, these involve chain interactions, free volume and intermolecular packing.[42] However, in the case of the polybenzoxazines, the density decreases upon crosslinking, as it is shown in the simulations and demonstrated by Ishida. Thus, the free volume argument seems insufficient to explain the high T_g of the cured benzoxazines. The high T_g of the polybenzoxazines

compared to other thermosets cannot be explained by a high crosslink density, since the crosslink density is higher in epoxy resins than in polybenzoxazines, as we have shown it in the network topology characterization. The proposed explanation for the unexpectedly high T_g of the benzoxazine thermosets is the presence of hydrogen bonds in the cured structures due to the formation of O–H groups during the crosslinking process, since hydrogen bonds are capable of decreasing the flexibility of a crosslinked network by blocking the rotational configurational changes and other segmental motions.[42]

It has been reported that both P-*p*PDA and 4EP-*p*PDA exhibit no significant thermal degradation during the crosslinking process. Therefore, it is possible to accurately compare the simulation and experimental results. The two monomers have a similar T_g value: 37 °C and 47 °C for P-*p*PDA and 4EP-*p*PDA respectively. However, the difference increases drastically for partially and fully crosslinked structures, up to about 70 °C in the fully cured systems (see Fig. 8). We find that the volume increase during curing remains very similar (2.45% and 2.57% for P-*p*PDA and 4EP-*p*PDA, respectively), which suggests that the difference in T_g is not due to a difference in the free volume.

In order to evaluate the role of hydrogen bonding in the thermostability of these polybenzoxazines, the H bond density was measured for both resins at a 90% conversion rate. The formation of the H bonds is considered when the distance between a donor –OH and an acceptor –O or –N is less than 0.25 nm and the angle between –OHO and –OHN is between 120° and 180° degrees, as defined by Kim and Mattice.[22] The values were averaged over 5 frames in the last 100 ps of the MD simulations for five different types of H bonds (Table 2). Concerning the nature of the H bonds, the proportion of the H–N *vs.* H–O bonds is almost the same in the two resins; however, 50% of the H–N bonds are involved in six-membered ring intramolecular H-bonds, while such intramolecular H bonding is not observed with the H–O bonds. In addition, a few OH–π bonds are formed; they correspond to the interaction between an O–H group and the center of a benzene ring, which acts as a hydrogen bond acceptor.

The simulations indicate that the density of the H bonds is higher for P-*p*PDA; these additional intermolecular interactions can result in a higher stability of the structure and a higher T_g value for this resin. This higher stability is confirmed by the data in Fig. 9 showing a higher density of the hydrogen bond energy in the fully cured P-*p*PDA compared to 4EP-*p*PDA.

In the case of BA-a, T_g increases from 74 to 200 °C upon curing; this final value is overestimated in comparison with the experimental data, as the T_g of BA-a resin is measured to
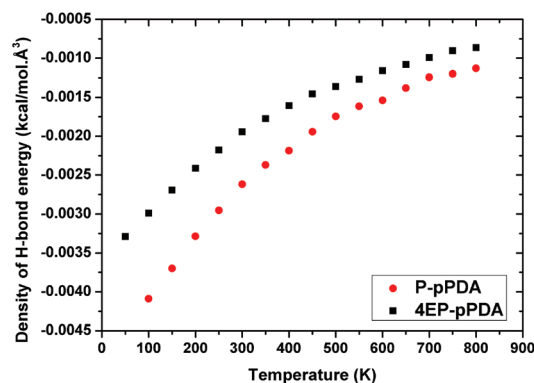

Fig. 9 Density of the hydrogen bond energy as a function of the temperature in P-*p*PDA and 4EP-*p*PDA structures crosslinked at a 90% conversion rate.

be between 150 and 170 °C.[42,43] However, it is important to point out that, in contrast to P-*p*PDA and 4EP-*p*PDA, a partial thermal degradation takes place during the curing of the BA-a resin, leading to the formation of a secondary volatile species. This degradation process may be responsible for a decrease of T_g in the actual system with respect to the ideal situation described in the simulations.

The calculated evolution of T_g upon crosslinking can be fitted by Di Benedetto's equation, which has been extensively used to describe the relation between T_g and the degree of conversion:[44]

$$\frac{T_g - T_g^0}{T_g^\infty - T_g^0} = \frac{\lambda \xi}{1 - (1 - \lambda)\xi} \tag{10}$$

where λ is an adjustable parameter that describes the non-linearity in the curve, ξ is the degree of conversion, T_g^0 and T_g^∞ are the glass transition temperatures for conversions of 0 and 100%, respectively. In the three benzoxazines studied here, we find that up to 70% conversion excellent agreement is obtained between the T_g evolution predicted by numerical simulations and from Di Benedetto's model (see Fig. 8). However, at higher conversions, the calculated T_g values start deviating from the model and tend to saturate. This saturation can be directly related to the fate of the structural defects in those resin systems: as shown in Fig. 4 and 5, above 80% conversion, the number of dangling, loop and free chains becomes very small and the resins are almost completely composed of elastic chains. At this point, the crosslink density reaches saturation and so does the glass transition temperature.

Table 2 The density of hydrogen bonds and π–π interactions for P-*p*PDA and 4EP-*p*PDA at 90% conversion

$\times 10^{-3}$ mol cm^{-3}	Total H-bonds	H–N	H–O	Intra H–N	Intra H–O	OH-p
P-*p*PDA	2.60 ± 0.10	1.29 ± 0.10	1.19 ± 0.10	0.66 ± 0.04	0	0.11 ± 0.04
4EP-*p*PDA	1.90 ± 0.06	0.95 ± 0.04	0.93 ± 0.04	0.52 ± 0.06	0	0.02 ± 0.01

From the fitting of the T_g evolution between 0 and 70% conversions, three different T_g regions can be identified: (i) the pregel linear regime, (ii) the postgel linear regime, which shows a larger slope and (iii) the non-linear regime, with T_g converging to its maximal value. The least squares method is applied in order to fit the simulation curves; the calculated values are represented in Table 3. λ has been related to the ratio of the change of the heat capacity at T_g for fully cured and uncured structures: $\lambda = \Delta C_{100}/\Delta C_0$.[39]

The room temperature α_v coefficients for cured (90%) resins are presented in Table 4. The obtained results are in line with the published values for epoxy resins, which are in the range of $1.7–2.8 \times 10^{-4}$ K^{-1}. Nevertheless, the α_v coefficients of these benzoxazines are lower for epoxies, indicating a superior glass transition temperature for polybenzoxazines. The value calculated for BA-a $\sim1.67 \times 10^{-4}$ K^{-1} is very close to the experimental result 1.7×10^{-4} K^{-1}.[42] Below T_g, P-pPDA is clearly the most thermostable among the three resins, which can be useful not only in terms of thermal tenacity but also in terms of dimensional stability for various industrial applications.

Fig. 10 shows the calculated and experimental T_g as a function of the measured crosslinked density. All curves exhibit a linear behaviour, in line with previous reports on various epoxy and phenolic resins.[45,46] The experimental T_g for fully cured P-pPDA of ~220 °C is found to be identical to the value calculated for the maximal crosslink density. The experimental value for the 4EP-pPDA resin (~150 °C) is also in excellent agreement with our predicted value for the maximum crosslink density: ~147 °C. In the case of BA-a, two different T_g values have been reported in the literature: 150 and 170 °C; the corresponding measured crosslink densities are 1.1 and 1.95 ($\times10^{-3}$ mol cm^{-3}), respectively. These two values are also very close to the linear fit of our simulation results. This indicates that the partial thermal degradation of BA-a during curing reduces the number of the available functional groups, causing the decrease of the crosslink density, which in turn affects the thermomechanical properties. If one could suppress these degradation reactions, the experimental T_g of BA-a would increase up to ~205 °C, as predicted by our model for the maximal crosslink density.
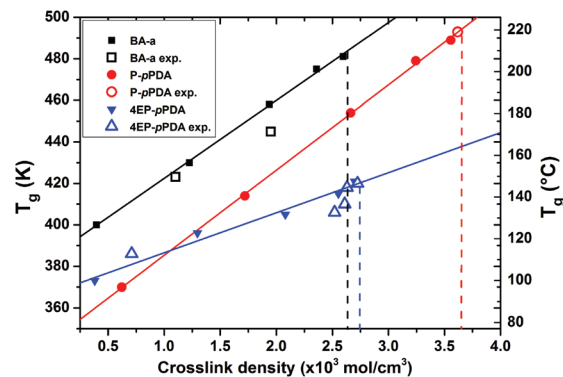

Fig. 10 Glass transition temperature as a function of the crosslink density for BA-a (black line and data points), P-pPDA (red line and data points) and 4EP-pPDA (blue line and data points). The full (open) data points correspond to the simulations (experimental measurements). Experimental data are extracted from ref. 5, 42 and 43.

3.3 Elastic properties

Two approaches can be followed to determine the mechanical properties from molecular modeling simulations. The first one is a dynamic approach that includes entropy effects. The second approach is the static constant-strain method, which has been used in this work (the simulation details are described in section 2).[47] We have shown above that the cured polybenzoxazine structures are very close to ideal elastic networks for a high crosslink conversion (90%), and hence the thermal contributions ought to be negligible at high conversion thereby validating the use of a static approach. All the structures have been equilibrated at room temperature, which makes it possible to compare the simulation data and the experimental results obtained at that temperature.

To obtain the estimates of the elastic constants, we averaged the strain and shear results over all structures and all directions, as proposed by Theodorou and Suter.[40] The absolute values of the elastic constants are summarized in Table 5, together with their standard deviations. Overall, the figures calculated for the crosslinked benzoxazines are higher than for the majority of epoxy resins, ca. 2.7 GPa.[42] The Young's moduli of the P-pPDA and 4EP-pPDA resins (6.03 ± 0.57 and 5.83 ± 0.49 GPa, respectively) are similar, considering the standard

Table 3 Calculated T_g^∞ and λ values

	T_g^∞	Λ
BA-a	578 K	0.39
P-pPDA	770 K	0.20
4EP-pPDA	694 K	0.15

Table 4 Comparison between experimental and computed coefficients of volume thermal expansion (α_v, 10^{-4} K^{-1}) for structures with a 90% conversion rate

	BA-a	P-pPDA	4EP-pPDA
MD simulations	1.67 ± 0.03	1.49 ± 0.0641	1.76 ± 0.14
Measurements	1.7 (ref. 42)	—	—

Table 5 Mechanical properties of BA-a, P-pPDA and 4EP-pPDA resins for 90% conversion from MD simulations and comparison with the available experimental results (in italics)

	Simulation results (MPa) at 300 K		
	BA-a	P-pPDA	4EP-pPDA
Young's modulus, E	5.33 ± 0.61 *5.2* (ref. 42)	6.03 ± 0.57	5.83 ± 0.49
Shear modulus, G	2.08 ± 0.13 *2.2* (ref. 42)	2.25 ± 0.17	2.28 ± 0.10
Bulk modulus, B	4.62 ± 0.62	6.15 ± 0.35	5.36 ± 0.15
Poisson's ratio, υ	0.30 ± 0.06	0.33 ± 0.04	0.32 ± 0.04

deviation. For BA-a, this modulus is slightly lower (5.33 ± 0.61 GPa). The same trend is observed for the shear modulus: it is very similar in the P-*p*PDA and 4EP-*p*PDA resins, 2.25–2.28 GPa, respectively, and lower for BA-a, 2.08 GPa. Ree–Eying theory applied to polymers states that the plastic behaviour is related to the specific degrees of freedom in terms of molecular-scale motions in the network structure.[48] Thus, here one may conclude that the lower elastic properties of the BA-a resin can be related to the additional degrees of freedom induced by the higher number of the available conformations in the BA-a network chains, due to the presence of the central methyl groups and the terminal phenyl rings. The calculated Poisson's ratio for all the resins is in a reasonable range for polymer materials.

Fig. 11 displays the shear and Young's moduli as a function of the temperature for the fully cured structures. The decrease of elastic properties with temperature can be partitioned into a low-*T* glassy region and a high-*T* rubbery region, though the data are too scattered and the resolution too low to identify the exact transition temperatures. The variation of the elastic moduli as a function of the temperature is also related to the dependency between the elastic properties and the available degrees of freedom in the structures. At low temperatures some of degrees of freedom become restricted, and this decreases the overall capacity of the polymer matrix to absorb

the strain energy leading to the increase of the deformation resistance.[48]

The absolute values of the calculated elastic constants are in good agreement with the experimental results: the experimental elastic modulus for BA-a, obtained from the initial slope of the strain–stress curves, is ~5.2 GPa,[42] whereas DMA measurements provide values for the storage modulus in the range of 3–4 GPa.[4,49] For the P-*p*PDA the storage modulus is reported to be in the range of 4–5 GPa,[4,5] and no other experimental data are available yet. Ideally the Young's modulus is equal to the storage modulus, however, in reality the tests performed to measure these moduli are different. In the first case it is the stress–strain test (material is constantly stretched), whereas the other one is a dynamic test based on oscillations. The experimental storage moduli for both BA-a and P-*p*PDA show that the former has lower elastic properties than the latter, and this tendency is confirmed by the simulation results.

4 Conclusions

Molecular dynamics simulations have been performed to track the evolution of the molecular structure of P-*p*PDA, BA-a and 4EP-*p*PDA benzoxazines during curing. The structural characteristics, such as the gel fraction, the size of the largest fragment and the reduced weight-average degree of polymerization (RDP) calculated from the number average M_n and weight average M_w molecular weights were evaluated for each step of the crosslinking process. The gelation point was identified based on the appearance of the first elastically active chain in the structures and on the occurrence of a maximum in the RDP curve. The quantification of the crosslink density and the number of structural defects (dangling and loop chains) in the gel fraction was also obtained. All results were found to be in good agreement with the experimental data. The simulations show that at high conversion rates structural defects are healed and that a fully elastic network is formed.

The thermo-mechanical properties were next evaluated and compared to experiment when available. The glass transition temperature was calculated for different crosslink densities, along with the coefficient of thermal expansion and the elastic constants for the fully cured systems. Through the MD simulations, we gained a deeper insight into the molecular mechanisms responsible for the high thermostability of the BA-a, P-*p*PDA and 4EP-*p*PDA polybenzoxazines: the crosslink density, the amount of structural defects and the density of hydrogen bonds. The role of the structural defects in the thermal properties was also elucidated.

Experimentally, the P-*p*PDA thermoset has the highest glass transition temperature compared to BA-a and 4EP-*p*PDA resins. MD simulations yield T_g values for these materials in very good agreement with experiment and allow gaining a better insight into the molecular mechanisms at the origin of the thermomechanical response. In particular, we showed that the higher thermal stability of P-*p*PDA compared to 4EP-*p*PDA
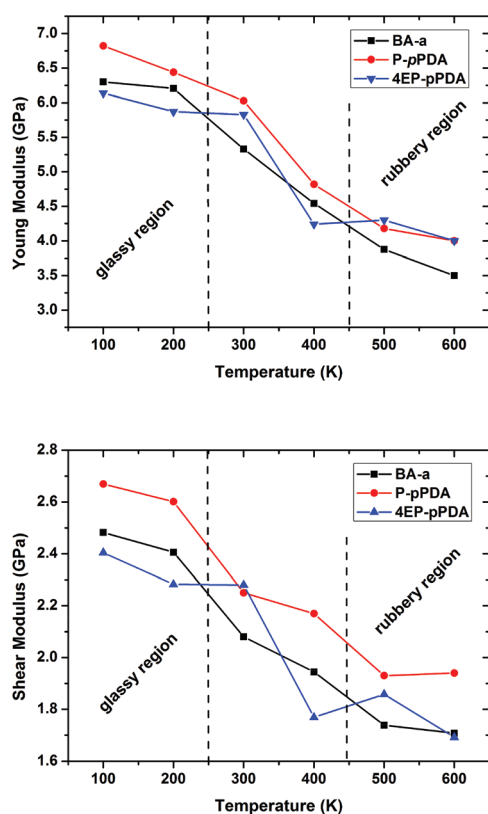

Fig. 11 The shear modulus and Young's modulus as a function of the temperature for BA-a, P-*p*PDA and 4EP-*p*PDA structures crosslinked at a 90% conversion rate.

is related to the higher density of hydrogen bonds in the cured structure. In addition, our calculations suggest that in the case of the BA-a thermoset thermal degradation of the resin while curing is the cause for the measured low T_g value.

This work highlights the ability of molecular dynamics simulations to efficiently explore the network topology and to predict with a good accuracy some of the thermomechanical properties of crosslinked benzoxazine thermosets. The methodology reported here offers the possibility to screen new benzoxazine thermosets as potential candidates for different industrial applications before synthesizing the molecules, a strategy we are now exploring further.

Conflicts of interest

There are no conflicts of interest.

Acknowledgements

Notes and references

1 X. Ning and H. Ishida, Phenolic materials via ring-opening polymerization: Synthesis and characterization of bisphenol-A based benzoxazines and their polymers, *J. Polym. Sci., Part A: Polym. Chem.*, 1994, **32**(6), 1121–1129.

2 N. N. Ghosh, B. Kiskan and Y. Yagci, Polybenzoxazines–new high performance thermosetting resins: synthesis and properties, *Prog. Polym. Sci.*, 2007, **32**(11), 1344–1391.

3 L. Dumas, L. Bonnaud, M. Olivier, M. Poorteman and P. Dubois, High performance bio-based benzoxazine networks from resorcinol and hydroquinone, *Eur. Polym. J.*, 2016, **75**, 486–494.

4 L. Dumas, L. Bonnaud, M. Olivier, M. Poorteman and P. Dubois, Facile preparation of a novel high performance benzoxazine-CNT based nano-hybrid network exhibiting outstanding thermo-mechanical properties, *Chem. Commun.*, 2013, **49**(83), 9543–9545.

5 L. Dumas, L. Bonnaud, M. Olivier, M. Poorteman and P. Dubois, High performance benzoxazine/CNT nanohybrid network-An easy and scalable way to combine attractive properties, *Eur. Polym. J.*, 2014, **58**, 218–225.

6 W. J. Burke, E. L. M. Glennie and C. Weatherbee, Condensation of Halophenols with Formaldehyde and Primary Amines1, *J. Org. Chem.*, 1964, **29**(4), 909–912.

7 W. J. Burke, J. L. Bishop, E. L. M. Glennie and W. N. Bauer Jr., A new aminoalkylation reaction. Condensation of phenols with dihydro-1, 3-aroxazines1, *J. Org. Chem.*, 1965, **30**(10), 3423–3427.

8 H. Ishida and D. P. Sanders, Regioselectivity of the ring-opening polymerization of monofunctional alkyl-substituted aromatic amine-based benzoxazines, *Polymer*, 2001, **42**(7), 3115–3125.

9 M. Schulz and H. L. Frisch, Monte Carlo studies of interpenetrating polymer network formation, *J. Chem. Phys.*, 1994, **101**(11), 10008–10022.

10 C. Wu and W. Xu, Atomistic molecular modelling of cross-linked epoxy resin, *Polymer*, 2006, **47**(16), 6004–6009.

11 C. Wu and W. Xu, Atomistic molecular simulations of structure and dynamics of crosslinked epoxy resin, *Polymer*, 2007, **48**(19), 5802–5812.

12 C. Li and A. Strachan, Molecular simulations of crosslinking process of thermosetting polymers, *Polymer*, 2010, **51**(25), 6058–6070.

13 J. S. Bermejo and C. M. Ugarte, Chemical crosslinking of PVA and prediction of material properties by means of fully atomistic MD simulations, *Macromol. Theory Simul.*, 2009, **18**(4–5), 259–267.

14 H. B. Fan and M. M. F. Yuen, Material properties of the cross-linked epoxy resin compound predicted by molecular dynamics simulation, *Polymer*, 2007, **48**(7), 2174–2178.

15 S. Yang and J. Qu, Computing thermomechanical properties of crosslinked epoxy by molecular dynamic simulations, *Polymer*, 2012, **53**(21), 4806–4817.

16 T. W. Sirk, K. S. Khare, M. Karim, J. L. Lenhart, J. W. Andzelm, G. B. McKenna and R. Khare, High strain rate mechanical properties of a cross-linked epoxy across the glass transition, *Polymer*, 2013, **54**(26), 7048–7057.

17 A. Bandyopadhyay, P. K. Valavala, T. C. Clancy, K. E. Wise and G. M. Odegard, Molecular modeling of crosslinked epoxy polymers: The effect of crosslink density on thermomechanical properties, *Polymer*, 2011, **52**(11), 2445–2452.

18 C. Li and A. Strachan, Evolution of network topology of bifunctional epoxy thermosets during cure and its relationship to thermo-mechanical properties: A molecular dynamics study, *Polymer*, 2015, **75**, 151–160.

19 X. Liu and Y. Gu, Molecular modeling of the chain structures of polybenzoxazines, *Chem. Res. Chin. Univ.*, 2002, **18**(3), 367–369.

20 S. A. Hall, I. Hamerton, B. J. Howlin and A. L. Mitchell, Validating software and force fields for predicting the mechanical and physical properties of poly (bisbenzoxazine) s, *Mol. Simul.*, 2008, **34**(10–15), 1259–1266.

21 G. R. Goward, D. Sebastiani, I. Schnell, H. W. Spiess, H.-D. Kim and H. Ishida, Benzoxazine oligomers: Evidence for a helical structure from solid-state NMR spectroscopy and DFT-based dynamics and chemical shift calculations, *J. Am. Chem. Soc.*, 2003, **125**(19), 5792–5800.

22 W.-K. Kim and W. L. Mattice, A fully atomistic model of an amorphous polybenzoxazine at bulk density, *Comput. Theor. Polym. Sci.*, 1998, **8**(3), 353–361.

23 W.-K. Kim and W. L. Mattice, Conformational statistics of a polybenzoxazine, *Comput. Theor. Polym. Sci.*, 1998, **8**(3), 339–351.

24 W.-K. Kim and W. L. Mattice, Molecular modeling of a thin film of polybenzoxazine, *Langmuir*, 1998, **14**(22), 6588–6593.

25 W.-K. Kim and W. L. Mattice, Static and Dynamic Behavior of H2O and O2 Penetrants in a Polybenzoxazine, *Macromolecules*, 1998, **31**(26), 9337–9344.

26 I. Hamerton, B. J. Howlin and A. L. Mitchell, Developing poly (bis-benzoxazines) with improved fracture toughness. 1: Using molecular simulation to determine and predict structure-property relationships, *React. Funct. Polym.*, 2006, **66**(1), 21–39.

27 S. Hall, I. Hamerton, B. Howlin, A. Mitchell and L. McNamara, Using Molecular Simulation to Predict the Physical and Mechanical Properties of Polybenzoxazines, *Handb. Benzoxazine Resins*, 2011, 127–142.

28 S. L. Mayo, B. D. Olafson and W. A. Goddard, DREIDING: a generic force field for molecular simulations, *J. Phys. Chem.*, 1990, **94**(26), 8897–8909.

29 J. Gasteiger and M. Marsili, Iterative partial equalization of orbital electronegativity–a rapid access to atomic charges, *Tetrahedron*, 1980, **36**(22), 3219–3228.

30 A. A. Samoletov, C. P. Dettmann and M. A. J. Chaplain, Thermostats for "slow" configurational modes, *J. Stat. Phys.*, 2007, **128**(6), 1321–1336.

31 B. Leimkuhler, E. Noorizadeh and O. Penrose, Comparing the efficiencies of stochastic isothermal molecular dynamics methods, *J. Stat. Phys.*, 2011, **143**(5), 921–942.

32 P. J. Flory, Molecular size distribution in three dimensional polymers. i. gelation1, *J. Am. Chem. Soc.*, 1941, **63**(11), 3083–3090.

33 P. J. Flory, Molecular size distribution in three dimensional polymers. II. Trifunctional branching units, *J. Am. Chem. Soc.*, 1941, **63**(11), 3091–3096.

34 P. J. Flory, Molecular size distribution in three dimensional polymers. III. Tetrafunctional branching units, *J. Am. Chem. Soc.*, 1941, **63**(11), 3096–3100.

35 A. M. Gupta, R. C. Hendrickson and C. W. Macosko, Monte Carlo description of A f homopolymerization: Diffusional effects, *J. Chem. Phys.*, 1991, **95**(3), 2097–2108.

36 L. Y. Shy, Y. K. Leung and B. E. Eichinger, Critical exponents for off-lattice gelation of polymer chains, *Macromolecules*, 1985, **18**(5), 983–986.

37 J. Scanlan, The effect of network flaws on the elastic properties of vulcanizates, *J. Polym. Sci.*, 1960, **43**(142), 501–508.

38 L. C. Case, Branching in polymers. I. Network defects, *J. Polym. Sci.*, 1960, **45**(146), 397–404.

39 C. Li, G. A. Medvedev, E.-W. Lee, J. Kim, J. M. Caruthers and A. Strachan, Molecular dynamics simulations and experimental studies of the thermomechanical response of an epoxy thermoset polymer, *Polymer*, 2012, **53**(19), 4222–4230.

40 D. N. Theodorou and U. W. Suter, Atomistic modeling of mechanical properties of polymeric glasses, *Macromolecules*, 1986, **19**(1), 139–154.

41 P. J. Flory, Molecular theory of rubber elasticity, *Polymer*, 1979, **20**(11), 1317–1320.

42 H. Ishida and D. J. Allen, Physical and mechanical characterization of near-zero shrinkage polybenzoxazines, *J. Polym. Sci., Part B: Polym. Phys.*, 1996, **34**(6), 1019–1030.

43 M. T. Huang, Dynamic Mechanical Analysis of Reactive Diluent Modified Benzoxazine-based Phenolic Resin, *Polym. Polym. Compos.*, 1999, **7**, 233–247.

44 L. E. Nielsen, Cross-linking-effect on physical properties of polymers, *J. Macromol. Sci., Chem.*, 1969, **3**, 69–103.

45 G. Levita, S. De Petris, A. Marchetti and A. Lazzeri, Crosslink density and fracture toughness of epoxy resins, *J. Mater. Sci.*, 1991, **26**(9), 2348–2352.

46 M. Ogata, N. Kinjo and T. Kawata, Effects of crosslinking on physical properties of phenol-formaldehyde novolac cured epoxy resins, *J. Appl. Polym. Sci.*, 1993, **48**(4), 583–601.

47 N. B. Shenogina, M. Tsige, S. S. Patnaik and S. M. Mukhopadhyay, Molecular modeling approach to prediction of thermo-mechanical behavior of thermoset polymer networks, *Macromolecules*, 2012, **45**(12), 5307–5315.

48 A. D. Mulliken and M. C. Boyce, Mechanics of the rate-dependent elastic-plastic deformation of glassy polymers from low to high strain rates, *Int. J. Solids Struct.*, 2006, **43**(5), 1331–1356.

49 C. Zúñiga, L. Bonnaud, G. Lligadas, J. C. Ronda, M. Galià, V. Cádiz and P. Dubois, Convenient and solventless preparation of pure carbon nanotube/polybenzoxazine nanocomposites with low percolation threshold and improved thermal and fire properties, *J. Mater. Chem. A*, 2014, **2**(19), 6814–6822.